Neutral atmospheric delay in interferometric synthetic aperture radar applications: Statistical description and mitigation

T. R. Emardson
Jet Propulsion Laboratory, California Institute of Technology, Pasadena, California, USA

M. Simons
Seismological Laboratory, Division of Geological and Planetary Sciences, California Institute of Technology, Pasadena, California, USA

F. H. Webb
Jet Propulsion Laboratory, California Institute of Technology, Pasadena, California, USA

Received 23 January 2002; revised 19 December 2002; accepted 31 January 2003; published 3 May 2003.

[1] Variations in the refractive index of the atmosphere cause variations in satellite-based interferometric synthetic aperture radar (InSAR) observations. We can mitigate tropospheric effects by averaging N-independent interferograms. Because the neutral atmosphere is uncorrelated at timescales longer than 1 day, using this technique statistically reduces the variance, σ^2, of the noise by a factor of N. Using zenith neutral atmospheric delays from Global Positioning System (GPS) data from the Southern California Integrated GPS Network, we find that the average variance depends on the distance between observations, L, and height difference, H, as $\sigma = c\,L^{\alpha} + kH$ with estimated values for c, α, and k of about 2.5, 0.5, and 4.8, respectively, where σ is in mm and L and H are in km. We expect that the value of α is largely site-independent but the value of c will depend on the water vapor variability of the area of interest. This model is valid over a range of L between approximately 10 and 800 km. Height differences between 0 and 3 km have been used in this analysis. For distances of 100 and 10 km with negligible height differences, σ is estimated to be approximately 25 and 8 mm, respectively. For a given orbit revisit time and image archive duration, we calculate the number and duration (assumed constant) of interferograms required to achieve a desired sensitivity to deformation rate at a given length scale. Assuming neutral atmosphere is the dominant source of noise, a 30° look angle, and an image revisit time of 7 days, detection of a deformation rate of 1 mm yr^{-1} over distances of 10 km requires about 2.2 years of continuous observations. Given our results, we suggest a data covariance structure to use when using InSAR data to constrain geophysical models. *INDEX TERMS:* 1206 Geodesy and Gravity: Crustal movements—interplate (8155); 1208 Geodesy and Gravity: Crustal movements—intraplate (8110); 1243 Geodesy and Gravity: Space geodetic surveys; 1244 Geodesy and Gravity: Standards and absolute measurements; 1294 Geodesy and Gravity: Instruments and techniques; *KEYWORDS:* radar interferometry, troposphere, InSAR, crustal deformation

Citation: Emardson, T. R., M. Simons, and F. H. Webb, Neutral atmospheric delay in interferometric synthetic aperture radar applications: Statistical description and mitigation, *J. Geophys. Res.*, *108*(B5), 2231, doi:10.1029/2002JB001781, 2003.

1. Introduction

[2] Interferometric synthetic aperture radar (InSAR) provides high resolution maps of both topography and surface deformation [*Zebker and Goldstein*, 1986; *Gabriel et al.*, 1989; *Massonnet and Feigl*, 1998; *Rosen et al.*, 2000]. The prime observable in InSAR is the phase difference between radar observations taken at different times and from slightly different orbital positions. A major source of noise is the unpredictable phase delay that occurs as radio waves propagate through the atmosphere. Under most circumstances these phase delays cannot be separated from the effect of topography and deformation.

[3] Several studies consider the effect on SAR interferograms caused by the signal delay in the atmosphere, especially the delay due to the neutral atmosphere, which is mainly confined to the troposphere. *Goldstein* [1995] considers the spatial power spectrum of observed interferometric data from the Mojave desert in California, and finds

0148-0227/03/2002JB001781$09.00

that most of the error is caused by water vapor turbulence, with a 2.4 mm root-mean-square (RMS) amplitude at spatial scales of 6 km and smaller. In a study of three interferograms at two different frequencies observed during a four-day period over Hawaii, *Zebker et al.* [1997] find RMS errors of up to 1 cm in two-pass measurements over small areas of the imaged swath. In a study over Mount Etna, *Beauducel et al.* [2000] analyze 238 interferograms to separate the effect of the neutral atmosphere from that of deformations by analyzing the correlation between pixel altitude and phase values.

[4] In these studies, the contribution of the atmospheric water vapor to the noise in the interferogram is inferred from spatially and temporally limited data. With the availability of data from continuous Global Positioning System (GPS) networks, we have the opportunity to investigate the statistical character of atmospheric water vapor at spatial and temporal scales that are commensurate with those in InSAR studies of deformation. One should keep in mind, however, that the GPS estimates are obtained by combining measurements over a reversed cone above the GPS receiver and that GPS networks cannot deliver atmospheric data at the pixel scale of InSAR.

[5] There are numerous assessments of the accuracy of the wet delay estimates from GPS from comparisons with independent techniques such as radiosondes and microwave radiometry [e.g., *Duan et al.*, 1996; *Emardson et al.*, 1998; *Tregoning et al.*, 1998]. The accuracy in the delay measurements is believed to be better than 1 cm for a zenith estimate. *Williams et al.* [1998] study spatial and structural variations of water vapor using GPS data from stations in southern California and discuss the potential effect on SAR interferograms of a troposphere that conforms temporally and spatially to a *Treuhaft and Lanyi* [1987] statistical model. *Williams et al.* [1998] also suggest that calibration of InSAR images can be performed using delay measurements from GPS using a statistical interpolator. The *Treuhaft and Lanyi* [1987] model relies on the assumption that the characteristics of the water vapor concentrations that can be derived from the Kolmogorov turbulence for small spatial scales is valid also for larger scales. It is unclear whether this model should be extrapolated to the length scales characteristic of InSAR observations.

[6] In the present study we are not aiming to model out the atmospheric effects from interferograms using GPS. Instead, we use estimates of the observed neutral delay from GPS observations in southern California to understand the behavior of the expected noise levels in SAR interferograms by examining the differential zenith tropospheric delay at different times between pairs of sites. This is analogous to the observing scenario of repeat orbit InSAR where observations are taken at two different times and the differential delay among points in the interferogram are compared.

2. Effect of the Neutral Atmosphere on SAR Interferograms

[7] We use data from 126 stations in the Southern California Integrated GPS Network (SCIGN) [*Hudnut et al.*, 1999] spanning the period from January 1998 to March 2000. The GPS observations are decimated to 5 min intervals and processed in 24 hour daily solutions using the GIPSY software [*Webb and Zumberge 1993*] and the precise point positioning technique [*Zumberge et al.*, 1997]. This technique is based on the use of pre-determined satellite orbits and clocks estimated from a global network and thereafter used in the estimation of the site specific parameters, such as the three-dimensional positions, stations clocks, and the neutral atmospheric delay. For each regional site, we estimate the positions as unconstrained constant values, the receiver clocks as white noise processes, and the zenith neutral atmospheric delays and atmospheric gradients as a random walk processes. We use no observations below an elevation angle of 15° in the solution.

[8] From GPS, we obtain one delay time series, $\ell_i(t)$, per site i. All time series are screened in order to remove delay estimates obviously in error, i.e., we remove estimates that are more than 0.5 m off from the mean value of that site. By forming the differences between all possible combinations of sites at a given time, t, we obtain

$$\delta\ell_{i,j}(t) = \ell_i(t) - \ell_j(t). \tag{1}$$

By choosing one value of $\delta\ell_{i,j}(t)$ per day at $t = t_n$, we can emulate an InSAR scenario with one scene observed per day. We can then simulate interferometric observations by differencing the values of $\delta\ell_{i,j}(t_n)$:

$$P_{i,j,m,n} = \delta\ell_{i,j}(t_n) - \delta\ell_{i,j}(t_m). \tag{2}$$

If we use the same time interval for all pairs, we can write the last time series as $P_{i,j,T}$, where T is $t_n - t_m$. If the time between observations is large enough, we can treat the time series P as uncorrelated and consisting of values P_k, where P_k lie in the set $\mathbf{P}_{L,T}$ and L is the distance between site i and site j. An analysis similar to the one described here has been presented by *Hanssen* [2001]. In order to facilitate comparisons with his analysis, $\delta\ell_{i,j}(t_n)$ in this study corresponds to $\delta_{qp}^{t_n}$ used by *Hanssen* [2001], where q and p are used instead of i and j, respectively.

[9] We assume here that for T greater than ~1 day, P_k is uncorrelated. Previous work suggests that this assumption is valid [e.g., *Jarlemark and Elgered*, 1998; *Emardson*, 1998]. Figure 1 shows the structure function, D, for three time series $\delta\ell(t)_{i,j}$, where D is defined as

$$D_{\delta\ell_{i,j}}(dt) = \left\langle \left[\delta\ell_{i,j}(t) - \delta\ell_{i,j}(t+dt)\right]^2 \right\rangle, \tag{3}$$

and the angle brackets indicate the expected value. D is often used for characterization of the temporal variation of water vapor [e.g., *Jarlemark and Elgered*, 1998, *Linfield et al.*, 1996]. From Figure 1, for T greater than ~1 day, D is relatively flat, indicating that our delay series are essentially temporally uncorrelated.

[10] In the context of InSAR analysis, we are interested in the variance, σ^2, of the interferograms. We can write the standard deviation as a function of the number of averaged interferograms, N, length scale, L, and height difference, H, between site(pixel) i and site(pixel) j, and time, T:

$$\sigma^2_{N,L,H,T} = \mathrm{Var}\left[\frac{1}{N}\sum P_k\right]. \tag{4}$$

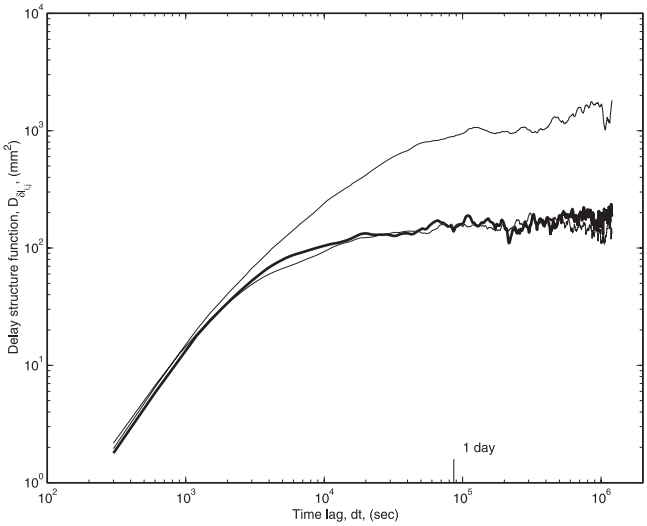

Figure 1. Structure function, $D_{\delta l_{i,j}}$ for the site pairs BRAN-MONP with a 224 km baseline (thin top curve), BRAN-DAM2 with 20 km baseline (thick middle curve), and PVEP-USC1 with 33 km baseline (thin bottom curve). See color version of this figure in the HTML.

We use data from the SCIGN network to form ~4000 estimates of σ^2 at different length scales (Figure 2), with N typically corresponding to ~800 GPS measurements at a given length scale. Because the values P_k are uncorrelated, σ is proportional to $1/\sqrt{N}$. Therefore, knowing σ as a function of L and T is sufficient to determine an expected variance in a number of stacked interferograms. Figures 2 and 3 show log σ as a function of log L and σ as a function of H for T equal to 7 days. We assume a relationship of the form

$$\sigma = cL^{\alpha} + kH, \tag{5}$$

where L and H are the differential length and height in km, respectively. Also shown in Figure 2 are estimates of the 90% confidence intervals estimated using a bootstrap procedure. From Table 1, we see that estimates of k are almost an order of magnitude larger for T greater than a day than for T equal to one day. This increase in k suggests that the mean vertical stratification of the troposphere remains correlated over longer times (greater than 1 day and less than 3 days) than horizontal variations which have correlation times of a day or less. The highest value of α is found for T = 6 months, presumably due to seasonal differences in the amount of atmospheric water vapor. Since our primary interest is in the use of interferograms with $T > 1$, for the remaining discussion we use $c = 2.5$ and $\alpha = 0.5$ as representative of long term interferograms and assume the dependence of σ on H is negligible. This assumption can be justified by Figures 2 and 3, where the dependence of σ on L is seen to be much larger than that of H for length scales greater than 10 km. *Hanssen* [2001] also investigates the relationship between σ and height differences using radiosonde data from De Bilt, Holland, and finds variations twice as large as those presented here. In addition to effects caused by differences in the relative climates, there may be effects due to differences in the sampling of the atmosphere in the different data sets. The California data set

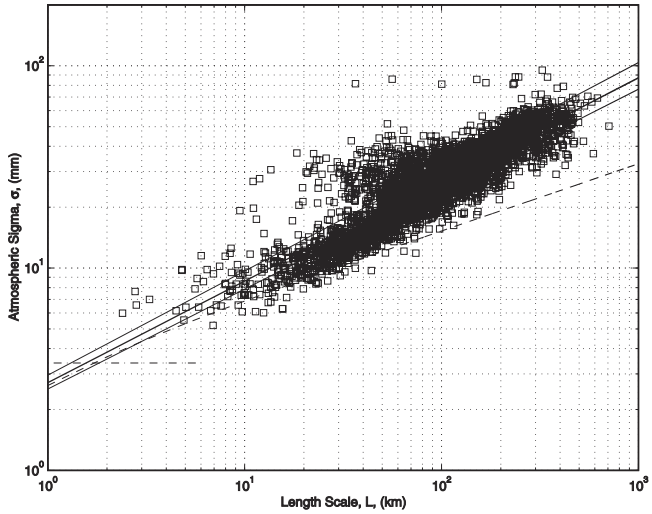

Figure 2. Atmospheric variance, σ, as a function of length scale L. The bold line represents the function $\sigma = cL^{\alpha} + kH$. The upper and lower thin lines show the corresponding fit to the 90% confidence limits. Theoretical values given by *Treuhaft and Lanyi* [1987] are shown as a dashed line. Values determined by *Goldstein* [1995] are shown as a dash-dotted line. See color version of this figure in the HTML.

presented here have much greater height differences and horizontal distances than in the Holland data set.

3. Stacking of Interferograms

[11] We wish to estimate the minimum deformation rate (assumed constant), $v_{\min}$, that can be resolved by stacking several interferograms. Given N-independent interferograms, we assume that the measured displacement, d_i, of a pixel in the ith interferogram can be written as

$$d_i = vT_i + e_i, \tag{6}$$

where v is the deformation rate, T_i represents the time period spanned by the particular interferogram, and e_i is zero mean

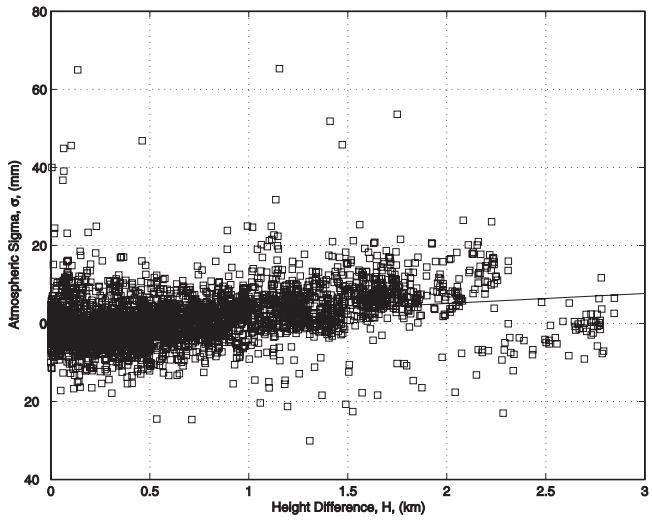

Figure 3. Atmospheric variance, σ, as a function of height difference with the length dependence removed. See color version of this figure in the HTML.

Table 1. Values of c, α, and k in Equation (5) Calculated for Different Values of T[a]

T	α	c	k	$C_{c\alpha}$	C_{ck}	$C_{\alpha k}$	Number of Data Points
1 day	0.44 ± 0.004	2.8 ± 0.1	0.5 ± 0.1	−0.979	−0.192	0.038	3968
3 days	0.48 ± 0.005	2.6 ± 0.1	3.4 ± 0.2	−0.981	−0.229	0.081	3998
7 days	0.50 ± 0.005	2.5 ± 0.1	4.8 ± 0.2	−0.982	−0.264	0.123	3995
14 days	0.51 ± 0.005	2.4 ± 0.1	5.5 ± 0.2	−0.982	−0.268	0.128	3894
1 month	0.49 ± 0.006	2.8 ± 0.1	4.5 ± 0.2	−0.982	−0.275	0.135	3779
3 months	0.51 ± 0.006	2.6 ± 0.1	4.9 ± 0.2	−0.983	−0.291	0.155	3329
6 months	0.59 ± 0.007	1.8 ± 0.1	5.5 ± 0.2	−0.988	−0.425	0.320	3069
12 months	0.54 ± 0.009	1.9 ± 0.1	5.7 ± 0.3	−0.988	−0.431	0.327	1614

[a]Also indicated are the correlation coefficients for the different parameters. These values correspond to σ in mm and L and H in units of km. Uncertainties are normalized so that $\chi^2 = 1$. Here each data point corresponds to a value on σ and is based on typically 800 GPS measurements from two sites.

measurement error with a variance of σ_i. In matrix notation we can write the expression as

$$\mathbf{d} = \Theta v + \mathrm{e}, \tag{7}$$

where

$$\Theta = \begin{bmatrix} T_1 \\ T_2 \\ T_3 \\ \vdots \\ T_N \end{bmatrix} \tag{8}$$

The covariance matrix of the least squares solution for v is

$$C_{\hat{v}} = \left(\Theta^T C^{-1} \Theta\right)^{-1}, \tag{9}$$

where C is the diagonal covariance matrix of $\mathbf{d}$. Defining the minimum detectable deformation rate to be when the signal equals the expected noise, $\sqrt{C_v}$, $v_{\min}$ is given by

$$v_{\min} = \sqrt{C_{\hat{v}}} = \left[\sum_{i=1}^{N} \left(\frac{T_i}{\sigma_i}\right)^2\right]^{-1/2}. \tag{10}$$

This is a rather crude definition but still a useful measure. If T_i and σ_i are constant, equation (10) can be simplified to

$$v_{\min} = \frac{\sigma}{T\sqrt{N}}. \tag{11}$$

Given the interferometric pairing scheme illustrated in Figure 4, the minimum time period, T_{obs}, required to make N interferograms with constant time separation, T, is by definition

$$T_{\mathrm{obs}} = (N-1)T_{\mathrm{orb}} + T, \tag{12}$$

where T_{orb} is the orbit revisit time, which we assume is constant. To determine both the number of interferograms and the time spanned by each interferogram, in order to detect a given deformation signal, we substitute equation (12) into equation (11) and set $\delta v_{\min}/\delta N = 0$, which results in

$$\hat{N} = \frac{T_{\mathrm{obs}} + T_{\mathrm{orb}}}{3T_{\mathrm{orb}}}, \tag{13}$$

where we choose $\hat{N}$ as the smallest integer greater than or equal to the optimal number and the hat denotes the optimal value. We also find

$$\hat{T} = \frac{2}{3}(T_{\mathrm{obs}} + T_{\mathrm{orb}}), \tag{14}$$

where $\hat{T}/T_{\mathrm{orb}}$ must also be integer-valued (greatest value smaller than or equal to $\hat{T}/T_{\mathrm{orb}}$). Substituting equations (12) and (13) in equation (11) gives

$$\hat{v}_{\min} = \frac{3\sqrt{3}}{2}\sigma\left(\frac{T_{\mathrm{orb}}}{(T_{\mathrm{obs}} + T_{\mathrm{orb}})^3}\right)^{\frac{1}{2}}, \tag{15}$$

which is then the minimum detectable deformation rate that can be measured as a function of measurement noise in each interferogram, total observation time, and time between scenes. Conversely, we can write T_{obs} as

$$\hat{T}_{\mathrm{obs}} = \left(\frac{27}{4}\frac{\sigma^2}{v_{\min}^2}T_{\mathrm{orb}}\right)^{1/3} - T_{\mathrm{orb}}. \tag{16}$$

Generally, σ can be decomposed as

$$\sigma^2 = \sigma_{NA}^2 + \sigma_{\mathrm{iono}}^2 + \sigma_{\mathrm{inst}}^2 + \sigma_{\mathrm{decor}}^2, \tag{17}$$

where σ_{NA} is the noise contribution from the neutral atmosphere, σ_{iono} is the contribution from the ionosphere,

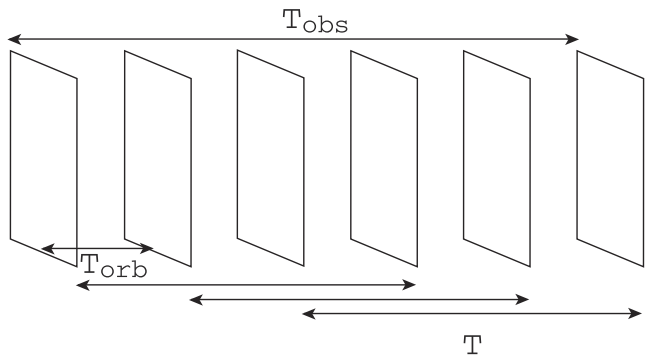

Figure 4. Description of the notation used. T_{obs} is the total time interval used for observations, T_{orb} is the time between SAR scenes, T is the time between scenes that form an interferogram. In this example T_{obs} is five units, T_{orb} is 1, T is 3, and the number of interferograms used in the stacking, N is 3.

σ_{inst} is instrumental noise, and σ_{decor} is errors due to interferometric decorrelation, [e.g., *Zebker and Villasenor*, 1992]. Assuming only noise from the neutral atmosphere, we can substitute equation (5) into equation (16) and obtain

$$\hat{T}_{obs} = \left(\frac{27}{4}\frac{\tilde{c}^2 L^{2\alpha}}{v_{min}^2} T_{orb}\right)^{1/3} - T_{orb}, \tag{18}$$

where $\tilde{c}$ corresponds to a rescaling of c to account for the difference in the slanted viewing geometry of InSAR. In this case, we assume that the difference in viewing geometry can be accounted for by scaling by a multiplicative constant $(\cos\gamma)^{-1}$, where γ is the line of sight incidence angle of the SAR observations and is typically between 20° and 40°. Here we assume $\alpha = 30°$, such that $\tilde{c} = 1.15c$. Similarly, from equation (15) we find

$$\hat{v}_{min} = \frac{3\sqrt{3}}{2}\tilde{c}L^{\alpha}\left(\frac{T_{orb}}{(T_{obs}+T_{orb})^3}\right)^{1/2}. \tag{19}$$

Figures 5 and 6 show $\hat{v}_{min}$ as a function of T_{obs} and L for T_{orb} equals 7 days.

[12] In the preceding analysis, N is integer valued. This limits the number of available solutions to the equations. Hence the above expressions should be viewed as a conservative estimate of what can be achieved through stacking of interferometric SAR data. In our derivation, v_{min} is with respect to a constant T. Under these assumptions, we do not use of all the observed scenes to effectively achieve v_{min}. Use of the remaining scenes will reduce $\hat{v}_{min}$. However, because the effective T for these few remaining scenes is much less than $\hat{T}$, they contribute only weakly to $\hat{v}_{min}$. For example, we consider a situation where $T_{obs} = 52$ weeks and $T_{orb} = 1$ week. In this case, there are 53 scenes with a maximum of independent interferograms, N_{max}, of 26.

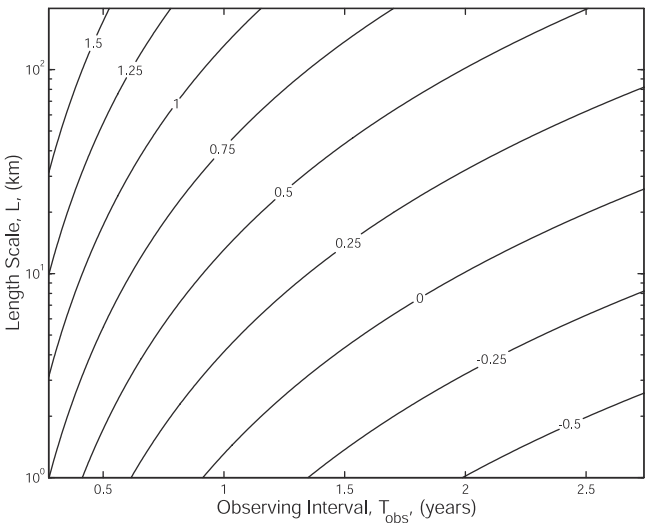

Figure 5. Minimum detectable deformation rate, v_{min}, as a function of T_{obs} and length scale, L, as calculated from equation (19). Contour labels are $\log_{10} v_{min}$, with v_{min} in units of mm/yr. T_{orb} is 7 days, and noise is assumed to come only from the neutral atmosphere; v_{min} is based on zenith measurements.

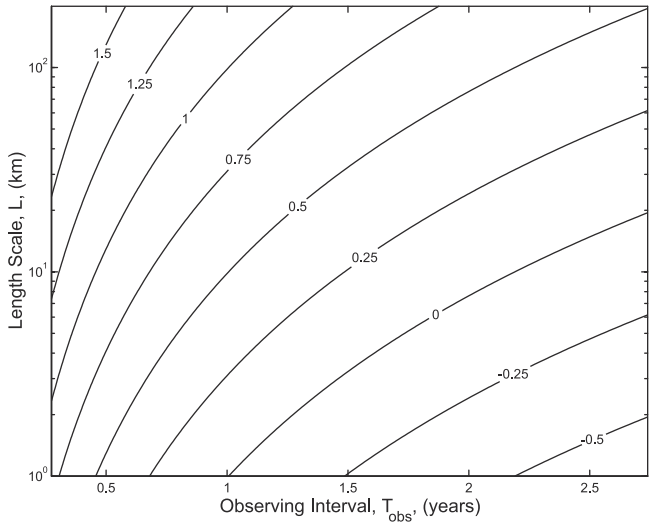

Figure 6. Same as Figure 5, but assuming a viewing geometry of 30° off zenith.

According to equation (13), the optimal number of interferograms, $\hat{N}$, is 18 and the optimal time span for each interferogram is 35 weeks. Using $\sigma = 1$ cm and equation (15) gives $\hat{v}_{min}$ of about 3.5 mm yr^{-1}.

[13] In this estimate, we have 8 independent interferograms that are unused. It is worth asking if our estimate of v_{min} would improve by supplementing our estimate with one or more of the unused interferograms. From equation (10), the supplemented v_{min} can be written as

$$v_{min} = \sqrt{\frac{\sigma^2}{NT^2 + T_e^2}}, \tag{20}$$

where T_e is the time spanned by the additional interferogram. The interferogram with the largest T_e (i.e., largest signal to noise ratio (SNR)) from the unused scenes spans 17 weeks. Equation (20) gives $v_{min} = 3.4$ mm yr^{-1}, improving the estimate only marginally.

4. Relationship Between σ and *D*

[14] The structure function is commonly used to investigate the spatial and temporal variability of water vapor (see equation (3)) and can be used to relate σ and the results presented here with previous studies of the neutral atmosphere. The spatial structure function is defined as

$$D(\mathbf{R}) = \left\langle [\ell(\mathbf{r}) - \ell(\mathbf{r}+\mathbf{R})]^2 \right\rangle, \tag{21}$$

where $\mathbf{r}$ is the location of one of the observations and $\mathbf{R}$ is the spatial vector between observation locations. Assuming one interferogram ($N = 1$), equation (4) gives

$$\sigma^2 = \mathrm{Var}[P_k] = \mathrm{Var}\left[\delta\ell_{i,j}(t_n) - \delta\ell_{i,j}(t_m)\right], \tag{22}$$

where the last equality is from equation (2). If the epochs t_m and t_n are sufficiently separated such that $\delta\ell_{i,j}(t_n)$ and $\delta\ell_{i,j}(t_m)$ are uncorrelated, we can write σ as

$$\sigma^2 = \mathrm{Var}\left[\delta\ell_{i,j}(t_n)\right] + \mathrm{Var}\left[\delta\ell_{i,j}(t_m)\right] = 2\mathrm{Var}[\delta\ell(t)]. \tag{23}$$

From equation (1), σ^2 can then be written as

$$\sigma^2 = 2\mathrm{Var}\left[\ell_i(t) - \ell_j(t)\right], \tag{24}$$

and if $\ell_i\,(t) - \ell_j\,(t)$ are zero mean,

$$\sigma^2 = 2E\left[\left(\ell_i(t) - \ell_j(t)\right)^2\right], \tag{25}$$

which is equal to the spatial structure function. Hence σ can be written as

$$\sigma = \sqrt{2D(\mathbf{R})}. \tag{26}$$

The structure function is often described using

$$D(\mathbf{R}) = gL^{\gamma}, \tag{27}$$

where $L = |\mathbf{R}|$ and g is a constant scaling factor similar to c. *Treuhaft and Lanyi* [1987] estimate a value for γ of 2/3 for L up to $O(10^3)$ km. For L much smaller than 1 km they estimate γ = 5/3, with a smooth transition between these length scales. The value of 5/3 can also be derived by integrating the structure function for the wet refractivity assuming a three dimensional turbulence [*Tatarskii*, 1971]. Using data from three continents *Emardson et al.* [2002] find values of γ in the range 0.8 to 1 for distances between 20 and 1000 km. *Hanssen* [2001] also finds values of γ close to 1 for structure functions computed using InSAR data over the Netherlands. Our estimate of $\alpha \approx 0.5$ corresponds to $\gamma \approx 1$.

5. Application

[15] A primary purpose of this study is to describe the observation requirements for InSAR to achieve given geodetic measurement goals. We can also use the results found herein to describe the data covariance matrix one should use when conducting parametric geophysical models using InSAR data. Such models include estimating the distribution of slip associated with earthquakes, the rheological parameters controlling postseismic deformation, the depths and geometry of magma chambers, and the rheology of glacier ice. A related discussion is given by *Williams et al.* [1998] and *Hanssen* [2001].

[16] Typically, when inverting InSAR data, we assume a given variance and that pixels within a given interferogram are uncorrelated. On the basis of the analysis presented here, the assumption of uncorrelated data is clearly incorrect and is primarily dependent on the relative distance between the pixels/observations, with a weak dependence on relative height. A complete analysis using multiple interferograms would include a data covariance containing the length (and height) dependence for pixels within a given interferogram as well as potential correlations associated with using interferograms with common radar scenes.

[17] If, given M scenes, no common scenes are used, then each interferogram can be considered as independent (assuming $T_{\mathrm{orb}} > 1$ day). The data covariance would then be block diagonal, with each block, C^{ij}, corresponding to each interferogram formed between epoch i and epoch j. For example, if scenes are formed between adjacent pairs in a time series, C would be given by

$$C = \begin{bmatrix} C^{12} & 0 & .. & 0 \\ & C^{34} & 0 & 0 \\ & & .. & 0 \\ & & & C^{(M-1)M} \end{bmatrix}, \tag{28}$$

where each C^{ij} contains the spatial correlations between pixels in the same interferogram due the atmosphere, orbit errors, ionosphere, etc. (Note when a matrix is symmetric, we use the convention of only writing the upper triangular portion.) See also *Hanssen* [2001] for a general discussion on the subject.

[18] Assuming that there is only an atmospheric contribution and that each interferogram is the same size ($p \times q$) and contains the same spatial distribution of observations, we can write equation (28) as

$$C = \begin{bmatrix} C^s & 0 & .. & 0 \\ & C^s & 0 & 0 \\ & & .. & 0 \\ & & & C^s \end{bmatrix}. \tag{29}$$

[19] C^s is then $pq \times pq$ with diagonal elements of σ_e^2 and off diagonal elements between any two pixels within a given interferogram given by

$$\begin{aligned} C^s_{12} &= \mathrm{Cov}(e_1, e_2) = \frac{1}{2}\mathrm{Var}[e_1] + \frac{1}{2}\mathrm{Var}[e_2] - \frac{1}{2}\mathrm{Var}[e_1 - e_2] \\ &= \sigma_e^2 - \frac{1}{2}\mathrm{Var}[e_1 - e_2], \end{aligned} \tag{30}$$

where e_1 and e_2 are the observation errors corresponding to the observations d_1 and d_2 and σ_e^2 is defined as $\mathrm{Var}[e] = \frac{1}{2}\mathrm{Var}[e_1] + \frac{1}{2}\mathrm{Var}[e_2]$. A typical value of σ_e can be determined from a large set of measurements assuming isotropy, homogeneity, and ergodicity. On the basis of the data set used here, we find $\sigma_e \approx 50$ mm. From equation (22), we find

$$C^s_{12} = \sigma_e^2 - \frac{1}{2}\sigma^2 = \sigma_{12}^2. \tag{31}$$

According to the results in this paper, for L between 10 and 500 km and assuming small height variations, σ^2 can be described as

$$\sigma = cL^{\alpha}. \tag{32}$$

Given σ_e = 50 mm, we find that the water vapor variations are uncorrelated at distances greater than ~800 km. This distance lies within the water vapor decorrelation range of 500–1000 km presented by *Emardson et al.* [2002] based on GPS data from Japan and radiosonde data from Europe. Similarly, for shorter distances, equation (32) is not valid. As described in section 4, $\gamma \approx 5/3$ for distances much shorter than 1 km. Hence, for those scales we can write

$$\sigma = cL^{\beta}, \tag{33}$$

where $\beta = \gamma/2 \approx 5/6$.

[20] In practice, the interferograms may not be independent. Lack of interferometric coherence between optimally

space scenes may require that interferograms be formed that have a common scene. In these cases, the correlation introduced by using the common scene will need to be accounted for in the parameter estimation in order to ensure that the values of the estimated parameters depend on the observations and not on how the scenes were selected that form the interferograms.

[21] For example, if two interferograms are formed from three independent data takes, i, j, and k, with i used as the common scene, then the line-of-sight, ρ, observations at any given pixel would be formed by

$$\mathbf{d} = \begin{bmatrix} \Delta\rho^{ij} \\ \Delta\rho^{ik} \end{bmatrix} = \begin{bmatrix} \rho^j - \rho^i \\ \rho^k - \rho^i \end{bmatrix}. \tag{34}$$

The variances for these observations are defined as

$$\mathrm{Var}\left[\Delta\rho^{ij}\right] = E\left[\left(\rho^i - \rho^j\right)^T\left(\rho^i - \rho^j\right)\right] \tag{35}$$

$$\mathrm{Var}\left[\Delta\rho^{ij}\right] = \sigma_i^2 + \sigma_j^2 \tag{36}$$

and the covariances as

$$\mathrm{Cov}\left[\Delta\rho^{ij}, \Delta\rho^{ik}\right] = E\left[\left(\rho^i - \rho^j\right)^T\left(\rho^i - \rho^k\right)\right] \tag{37}$$

$$\mathrm{Cov}\left[\Delta\rho^{ij}, \Delta\rho^{ik}\right] = \sigma_i^2. \tag{38}$$

The covariance matrix for these temporally differential observations is then

$$C^t = \begin{bmatrix} \sigma_i^2 + \sigma_j^2 & \sigma_i^2 \\ & \sigma_i^2 + \sigma_k^2 \end{bmatrix}. \tag{39}$$

If $\sigma_i^2 = \sigma_j^2 = \sigma_k^2 = \frac{1}{2}\sigma_e^2$, then this simplifies to

$$C^t = \sigma_e^2 \begin{bmatrix} 1 & \frac{1}{2} \\ & 1 \end{bmatrix}. \tag{40}$$

[22] For any pair of pixels, 1 and 2, observed at times i, j, and k as described previously, in the interferogram the observation vector, $\mathbf{d}$, is

$$\mathbf{d} = \begin{bmatrix} \rho_1^j - \rho_1^i \\ \rho_2^j - \rho_2^i \\ \rho_1^k - \rho_1^i \\ \rho_2^k - \rho_2^i \end{bmatrix}. \tag{41}$$

The form of the correlation matrix for these spatially and temporally correlated observations would contain terms for the spatial correlations, $C_{12}^{ij} = C_{12}^{ik} = C^s$, on the diagonal, and temporal and spatial correlations, $C_{12}^{ijk} = C^{t,s}$ on the off diagonal

$$C_{12} = \begin{bmatrix} C^s & C^{t,s} \\ & C^s \end{bmatrix} \tag{42}$$

$$C_{12} = \begin{bmatrix} \sigma_e^2 & \sigma_{12}^2 & \frac{1}{2}\sigma_e^2 & \frac{1}{2}\sigma_{12}^2 \\ & \sigma_e^2 & \frac{1}{2}\sigma_{12}^2 & \frac{1}{2}\sigma_e^2 \\ & & \sigma_e^2 & \sigma_{12}^2 \\ & & & \sigma_e^2 \end{bmatrix}. \tag{43}$$

6. Discussion

[23] Propagation delays in the atmosphere are the dominant noise source for InSAR and may be the limiting error for future InSAR missions aimed at observing millimeters per year changes in the Earth's crust. Delays arising in the ionosphere may have small-scale variability and decorrelation times that are fundamentally different from the neutral atmosphere. However, in future missions, the effect of the ionosphere may be mitigated by deploying a dual frequency or split band radar system.

[24] For the neutral atmosphere, the statistics of its spatial and temporal variability suggest that image stacking may be a reasonable approach to mitigating its effects at time periods greater than 1 day. While this is not an issue for the current constellation of orbiting SAR satellites which have revisit times, T_{orb}, of one day or longer, it should be noted for future mission design studies that our analysis is facilitated by the use of uncorrelated data. At time intervals shorter than one day, the calculations and results would be different since the delays may be correlated. In addition, InSAR observations with time intervals shorter than one day can also occur in tandem satellite missions.

[25] Given the level of noise, correlation times, and spatial correlations in the neutral atmosphere, future InSAR missions may need to focus on observing scenarios that ensure a reasonably large set of interferograms. The period of observations necessary to achieve a given level of confidence in the deformation rate will depend on the length scale of the area investigated.

[26] This study shows that the standard deviation of the neutral atmosphere induced noise, σ, can be written as $\sigma = cL^{\alpha} + kH$, where for southern California typical values of c, α, and k are 2.5, 0.5, and 4.8, respectively. These results are consistent with structure function values reported from other areas of the world using GPS and radiosonde data [e.g., *Emardson et al.*, 1998]. It is expected that the value of α is largely site-independent but the value of c will depend on the water vapor variability of the area of interest. This expectation is supported by studies of structure functions using data from different areas of the Earth [*Emardson et al.*, 2002]. Since σ is proportional to $N^{-1/2}$, we find σ is given by $\sigma = \tilde{c}L^{\alpha}N^{-1/2}$ and the number of interferograms necessary to reduce the atmospheric noise below a certain level is $N = \tilde{c}^2 L^{2\alpha}\sigma^{-2}$.

[27] From equation (18), we can determine the length of observation time necessary to measure a given deformation rate. Constraints imposed by interferometric decorrelation may require using $T \neq \hat{T}$. In such cases, one can still use the preceding derivations to estimate T_{obs}, N, or v_{min}. Assuming the noise contribution from the neutral atmosphere is the dominant noise source and a viewing geometry of 30° off zenith, resolving a deformation rate of 1 mm yr^{-1} over distances of 10 km where scenes are 7 days apart would take 2.2 years. Resolving the same deformation over 100 km would take approximately 4.8 years. These types of observational requirements suggest that future InSAR missions which aim to monitor small scale and/or short duration crustal deformation will need to make observations that are obtained frequently and can be reliably interfered over relatively long time periods.

[28] **Acknowledgments.** The authors thank Ken Hurst for the processing of the GPS data and D. Dong and S. Wu for helpful discussion. We also thank K. Feigl, R. F. Hanssen, and F. Sigmundsson for constructive reviews. This research was in part supported by the Swedish Foundation for International Cooperation in Research and Higher Education (STINT) and performed at the Jet Propulsion Laboratory, California Institute of Technology, under contract with the National Aeronautics and Space Administration. We acknowledge the Southern California Integrated GPS Network and its sponsors, the W. M. Keck Foundation, NASA, NSF, USGS, and SCEC.

References

Beauducel, B., P. Briole, and J.-L. Foger, Volcano-wide fringes in ERS synthetic aperture radar interferograms of ETNA (1992–1998): Deformation or tropospheric effect?, *J. Geophys. Res.*, *105*, 16,391–16,402, 2000.

Duan, J., et al., GPS meteorology: Direct estimation of the absolute value of precipitable water, *J. Appl. Meteorol.*, *35*, 830–838, 1996.

Emardson, T. R., Studies of atmospheric water vapor using the Global Positioning System, *Tech Rep. 339*, Sch. of Electr. and Comput. Eng., Chalmers Univ. of Technol., Goteborg, Sweden, 1998.

Emardson, T. R., G. Elgered, and J. M. Johansson, Three months continuous monitoring of the atmospheric water vapor with a network of Global Positioning System receivers, *J. Geophys. Res.*, *103*, 1807–1820, 1998.

Emardson, T. R., F. H. Webb, and P. O. J. Jarlemark, Analysis of water vapor spatial variability using GPS InSAR, microwave radiometer, and radiosonde data, *JPL IOM 335-02-01-L*, Jet Propul. Lab., Pasadena, Calif., 2002.

Gabriel, A. K., R. M. Goldstein, and H. A. Zebker, Mapping small elevation changes over large areas: Differential radar interferometry, *J. Geophys. Res.*, *94*, 9183–9191, 1989.

Goldstein, R. M., Atmospheric limitations to repeat-track radar interferometry, *Geophys. Res. Lett.*, *22*, 2517–2520, 1995.

Hanssen, R. F., *Radar Interferometry: Data Interpretation and Analysis*, Kluwer Acad., Norwell, Mass., 2001.

Hudnut, K. W., Y. Bock, J. E. Galetzka, F. H. Webb, and W. H. Young, The Southern California Integrated GPS Network (SCIGN), in *Proceedings of the International Workshop on Seismotectonics at the Subduction Zone*, edited by Y. Fujinawa, pp. 175–196, Natl. Res. Inst. for Earth Sci. and Disaster Prevent., Tsukuba, Japan, 1999.

Jarlemark, P. O. J., and G. Elgered, Characterization of temporal variations in atmospheric water vapor, *IEEE Trans. Geosci. Remote Sens.*, *36*, 319–321, 1998.

Linfield, R. P., S. J. Keihm, L. P. Teitelbaum, S. J. Walter, M. J. Mahoney, R. N. Treuhaft, and L. J. Skjerve, A test of water vapor radiometer-based troposphere calibration using very long baseline interferometry observations on a 21-km baseline, *Radio Sci.*, *31*, 129–146, 1996.

Massonnet, D., and K. Feigl, Radar interferometry and its application to changes in the Earth's surface, *Rev. Geophys.*, *36*, 441–500, 1998.

Rosen, P. A., S. Hensley, I. R. Joughin, F. K. Li, S. N. Madsen, E. Rodriguez, and R. M. Goldstein, Synthetic aperture radar interferometry - Invited paper, *Proc. IEEE*, *88*, 333–382, 2000.

Tatarskii, V. I., The effects of the turbulent atmosphere on wave propagation, Israel Program for Sci. Transl., Jerusalem, 1971.

Tregoning, P., R. Boers, D. M. O'Brien, and M. Hendy, Accuracy of absolute precipitable water estimates from GPS observations, *J. Geophys. Res.*, *103*, 28,701–28,710, 1998.

Treuhaft, R. N., and G. E. Lanyi, The effect of the dynamic wet troposphere on radio interferometric measurements, *Radio Sci.*, *22*, 251–265, 1987.

Webb, F. H., and J. F. Zumberge, An introduction to the GIPSY/OASIS-II, *JPL Publ. D-11088*, Jet Propul. Lab., Pasadena, Calif., 1993.

Williams, S., Y. Bock, and P. Fang, Integrated satellite interferometry: Tropospheric noise, GPS estimates and implications for interferometric synthetic aperture radar products, *J. Geophys. Res.*, *103*, 27,051–27,067, 1998.

Zebker, H. A., and R. M. Goldstein, Topographic mapping from interferometric synthetic aperture radar observations, *J. Geophys. Res.*, *91*, 4993–4999, 1986.

Zebker, H. A., and J. Villasenor, Decorrelation in interferometric radar echoes, *IEEE Trans. Geosci. Remote Sens.*, *30*, 950–959, 1992.

Zebker, H. A., P. A. Rosen, and S. Hensley, Atmospheric effects in interferometric synthetic aperture radar surface deformation and topographic maps, *J. Geophys. Res.*, *102*, 7547–7563, 1997.

Zumberge, J. F., M. B. Heflin, D. C. Jefferson, M. M. Watkins, and F. H. Webb, Precise point positioning for the efficient and robust analysis of GPS data from large networks, *J. Geophys. Res.*, *102*, 5005–5017, 1997.

T. R. Emardson and F. H. Webb, Jet Propulsion Laboratory, California Institute of Technology, MS 238-600, 4800 Oak Grove Drive, Pasadena, CA 91109, USA. (ragne_emardson@space.se; fhw@jpl.nasa.gov)

M. Simons, Seismological Laboratory, California Institute of Technology, 252-21, Pasadena, CA 91125, USA. (simons@caltech.edu)